Differential approach to quantitative susceptibility mapping without background field removal

Tian Liu[1], Dong Zhou[2], Pascal Spincemaille[2], and Yi Wang[2]
[1]MedImageMetric LLC, New York, New York, United States, [2]Radiology, Weill Cornell Medical College, New York, New York, United States

PURPOSE. Background field removal is an important step in current quantitative susceptibility mapping (QSM)(1-4). However, high quality background field removal critically relies on phase unwrapping, skull stripping, and knowledge of the field boundary conditions, which are difficult to obtain in practice. In this work, we provide a theoretical analysis of the background field removal and propose a method to bypass these steps using a differential approach.

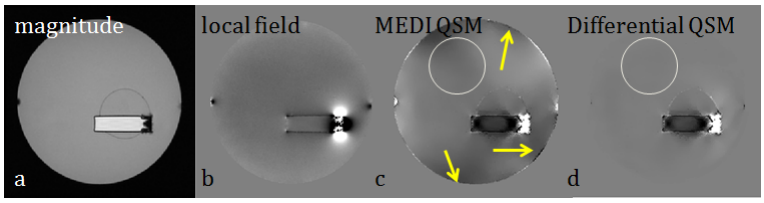

Fig. 1. Water phantom QSM.

THEORY. Current QSM approaches are based on the dipole convolution, $f = d * \chi$ (f field, d dipole kernel, and χ susceptibility distribution). This is the solution to Maxwell's Equations in the full space (R^3-space, susceptibility sources vanishing at ∞) that consists of the tissue region of interest Ω and the background (including regions of little or no signal). The determination of tissue susceptibility in Ω requires the removal of all background contributions to f (2,5), which is made difficult by the lack of knowledge of the boundary conditions of the Laplacian equation governing the background field behavior in Ω.

We have developed an alternative approach called differential QSM. Tissue susceptibility can be determined from its governing partial differential equation (PDE), $\nabla^2 f = (1/3\,\nabla^2 - \partial^2/\partial z^2)\chi$ in Ω (6). To connect with actual acquired MRI field data, consider the integral $\int_\Omega 1/|r-r'|\,\nabla^2 f(r')dr' \stackrel{\text{def}}{=} GMLf$, where G represents the convolution with kernel $1/r$, M is the binary mask corresponding to Ω with the surface removed,and $L = \nabla^2$ is the Laplacian. Taking the volume of integration to all of 3D space makes it equal to f. We therefore assume that the noise properties of $GMLf$ and f are the same. Then the data fidelity becomes $\left\|W(e^{-iGMLf} - e^{-iGMP\chi})\right\|_2^2$ with $GMP\chi \stackrel{\text{def}}{=} \int_\Omega 1/|r-r'|\,(1/3\,\nabla^2 - \partial^2/\partial z^2)\chi dr'$, where W is a noise whitening matrix calculated from echo time and signal amplitudes(7), and $P = (1/3\,\nabla^2 - \partial^2/\partial z^2)$. Since P is rank deficient, a regularization is used to penalize solutions not consistent with known anatomy as in morphology enabled dipole inversion (MEDI) (6,8-9). The Gauss-Newton method can be used to find $\chi^* = \text{argmin}_\chi \left\|W(e^{-iGMLf} - e^{-iGMP\chi})\right\|_2^2 + \lambda\|W_G\nabla\chi\|_1$. ($W_G$ is a binary mask with 0 for edges).

METHODS. The proposed differential QSM algorithm is compared with the MEDI method in a water phantom and healthy subjects (N=5). The water phantom was scanned using a 3D multi-gradient echo sequence on a 1.5T scanner (GE Excite HD) with a 5-inch surface coil for signal reception. The imaging parameters were TE/ΔTE /#TE/TR/FA/BW/FOV/matrix size=3.1ms/3.1ms/10/52.3ms/15°/±62.5kHz/$24 \times 24 \times 9.6\text{cm}^3$/$256 \times 256 \times 80$. Five healthy volunteers were scanned on a 3T scanner (GE Excite HD) under approval by the IRB. Imaging parameters were TE/ΔTE/#TE/TR/FA/BW/FOV/matrix size = 5ms/5ms/8/50ms/20°/±62.50kHz/$21.8 \times 24 \times 12.8\text{cm}^3$/$232 \times 256 \times 64$.

One advantage of the differential QSM method is that it does not require additional spatial phase unwrapping, as the finite difference implementation of $\nabla^2 f$ allows corrections of 2π multiples to ensure differences between neighboring voxels are in $(-\pi, \pi]$. Although excluding pure noise in signal void regions is still beneficial, skull stripping commonly used in current QSM methods is not required, which allows inclusion of more anatomical regions. In this example, all voxels with signal intensities greater than 10% of maximum signal intensity in the magnitude image were included.

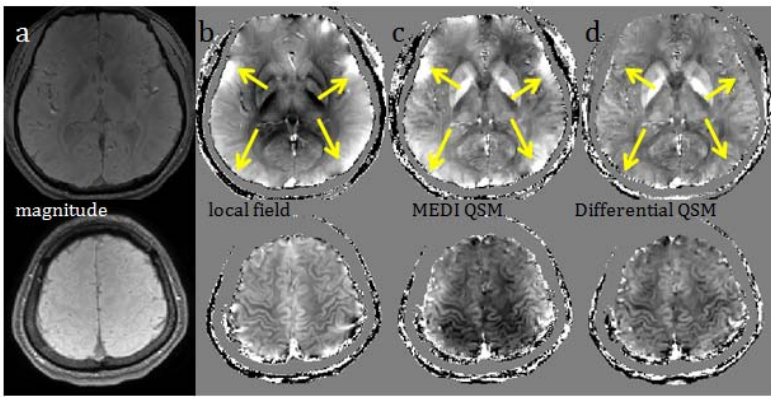

Fig. 2. Human head QSM.

RESULTS. The phantom results are shown in FIG. 1. It showed that even when minimal remnant background field was presented in the local field (Fig. 1b), large signal variation still appeared from the boundary of the region of interest using the reference method (arrows in Fig. 1c). This artifact was eliminated by the differential formulation (Fig. 1d). Quantitatively, the signal standard deviation measured in the homogenous phantom water region (white circle in Fig. 1c) was 0.0093ppm in Fig. 1c and 0.0023ppm in Fig. 1d. The human brain imaging results are shown in Fig. 2. It is demonstrated that remnant background field (arrows in Fig. 2b) led to artifacts in MEDI reconstructed QSM (Fig. 2c) and was suppressed in the differential method (arrows and circles in Fig. 2d).

DISCUSSION. When background field is poorly estimated, the differential QSM is superior to current QSM. This is especially apparent near air tissue interfaces, where current QSM has resorted to ROI erosion by removing voxels with poorly estimated local field. Both current and differential QSMs provide similar susceptibility mapping in regions far from ROI boundaries. Differential QSM may be preferred for mapping the cortex, superior sagittal sinus and other brain surface regions. When combined with fat-water separation, the differential QSM may allow mapping of susceptibility in the body.

CONCLUSION. A differential QSM method is developed based on the partial differential equation connection between susceptibility and the measured field. Differential QSM does not require additional spatial phase unwrapping, skull stripping, or background field removal, opening up a wider range of applications and anatomies for QSM.

REFERENCE. 1.Liu, T et al. Magn Reson Med 2009;61(1):196-204; 2.Schweser, F et al. Neuroimage 2011;54(4):2789-807; 3.Shmueli, K et al. Magn Reson Med 2009;62(6):1510-22; 4.Wharton, S et al. Magn Reson Med 2010;63(5):1292-304; 5.Liu, T et al. NMR Biomed 2011;24(9):1129-36; 6.de Rochefort, L et al. Magn Reson Med 2010;63(1):194-206; 7.Kressler, B et al. Ieee Transactions on Medical Imaging 2010;29(2):273-81; 8.Liu, J et al. Neuroimage 2012;59(3):2560-8; 9.Liu, T et al. Magn Reson Med 2013;69(2):467-76.